

Published in final edited form as:  
*Curr Biol.* 2017. DOI:

## Altered structural connectivity of the left visual thalamus in developmental dyslexia

Christa Müller-Axt<sup>1,\*</sup>, Alfred Anwander<sup>2</sup>, Katharina von Kriegstein<sup>1,3,4</sup>

<sup>1</sup> Research Group Neural Mechanisms of Human Communication, Max Planck Institute for Human Cognitive and Brain Sciences, Leipzig, Germany

<sup>2</sup> Department of Neuropsychology, Max Planck Institute for Human Cognitive and Brain Sciences, Leipzig, Germany

<sup>3</sup> Department of Psychology, Humboldt University of Berlin, Berlin, Germany

<sup>4</sup> Faculty of Psychology, Technical University of Dresden, Dresden, Germany

\* Corresponding author:

Christa Müller-Axt

Max Planck Institute for Human Cognitive and Brain Sciences

Research Group Neural Mechanisms of Human Communication

Stephanstr. 1a, 04103 Leipzig, Germany

Phone: +49 341 9940-2306

Email: [muelleraxt@cbs.mpg.de](mailto:muelleraxt@cbs.mpg.de)

<http://www.cbs.mpg.de/employees/muelleraxt>

## Summary

Developmental dyslexia is characterized by persistent reading and spelling deficits [1]. Partly due to technical challenges with investigating subcortical sensory structures, current research on dyslexia in humans by-and-large focuses on the cerebral cortex [2, 3]. These studies found that dyslexia is typically associated with functional and structural alterations of a distributed left-hemispheric cerebral cortex network [e.g., 4, 5]. However, findings from animal models and post-mortem studies in humans suggest that developmental dyslexia might also be associated with structural alterations in subcortical sensory pathways [6-12, reviewed in ref. 13]. Whether these alterations also exist in developmental dyslexia in-vivo and how they relate to dyslexia symptoms is currently unknown. Here we used ultra-high resolution structural magnetic resonance imaging (MRI), diffusion MRI and probabilistic tractography to investigate the structural connections of the visual sensory pathway in dyslexia in-vivo. We discovered that individuals with developmental dyslexia have reduced structural connections in the direct pathway between the left visual thalamus (LGN) and left middle temporal area V5/MT, but not between the left LGN and left primary visual cortex (V1). In addition, left V5/MT-LGN connectivity strength correlated with rapid naming abilities – a key deficit in dyslexia [14]. These findings provide the first evidence of specific structural alterations in the connections between the sensory thalamus and cortex in developmental dyslexia. The results challenge current standard models and provide novel evidence for the importance of cortico-thalamic interactions in explaining dyslexia.

**Keywords:** diffusion MRI, tractography, lateral geniculate nucleus (LGN), developmental dyslexia, primary visual cortex (V1), middle temporal area (V5/MT), rapid automatized naming (RAN), thalamus, DTI

## Results and Discussion

It is a long-standing, but untested, hypothesis that histological alterations of the visual sensory thalamus (i.e., the lateral geniculate nucleus, LGN), as found in dyslexics post-mortem, would be associated with alterations in the structural connections of the visual pathway [6]. However, to date there is no study that has yet examined the structural connections of the LGN in individuals with dyslexia. The reason is that the LGN's small size and deep position within the brain make it difficult to spatially map the LGN using noninvasive imaging techniques. Here we overcame this challenge by using ultra-high resolution 7 Tesla MRI quantitative  $T_1$  maps to individually delineate the LGN in a group of dyslexic adults ( $n=12$ , Table S1) and matched control participants ( $n=12$ , Table S1) (Figure 1A). We particularly focused on the LGN in the left hemisphere given evidence that dyslexia is associated with functional and structural alterations particularly of left-hemispheric regions [15, 16, reviewed in ref. 2].

The LGN segmentation procedure resulted in an average left LGN volume of  $119 \pm 22$  mm<sup>3</sup> in controls and  $114 \pm 19$  mm<sup>3</sup> in dyslexics, which is in good agreement with the average volume of 115 mm<sup>3</sup> that has been previously measured for the left LGN in post-mortem human specimens [17]. The group average maps of the LGN masks in standard space showed a high consistency in anatomical LGN location across participants (Figure 1B; see Supplemental Experimental Procedures).

To test the hypothesis that developmental dyslexia is associated with reduced structural connections between cerebral cortex areas and the LGN, we targeted two white matter pathways: (i) the structural white matter connections between the LGN and primary visual cortex (V1), as these connections constitute the major cortico-subcortical fibre pathway of the visual system [18] and (ii) the structural white matter connections between the LGN and middle temporal area V5/MT. Area V5/MT has direct V1-bypassing connections with the LGN [19-26] and has frequently been implicated in dyslexia in the context of dorsal visual stream dysfunction [reviewed in ref. 27]. We derived the left V1 and V5/MT masks from a volume-based probabilistic atlas (Juelich Histological Atlas; see Supplemental Experimental Procedures). Both the V1-LGN (Figure 2A) and the V5/MT-LGN (Figure 2B) connection could be reliably reconstructed by probabilistic tractography (see Supplemental Experimental Procedures) in all participants ( $N=24$ ).

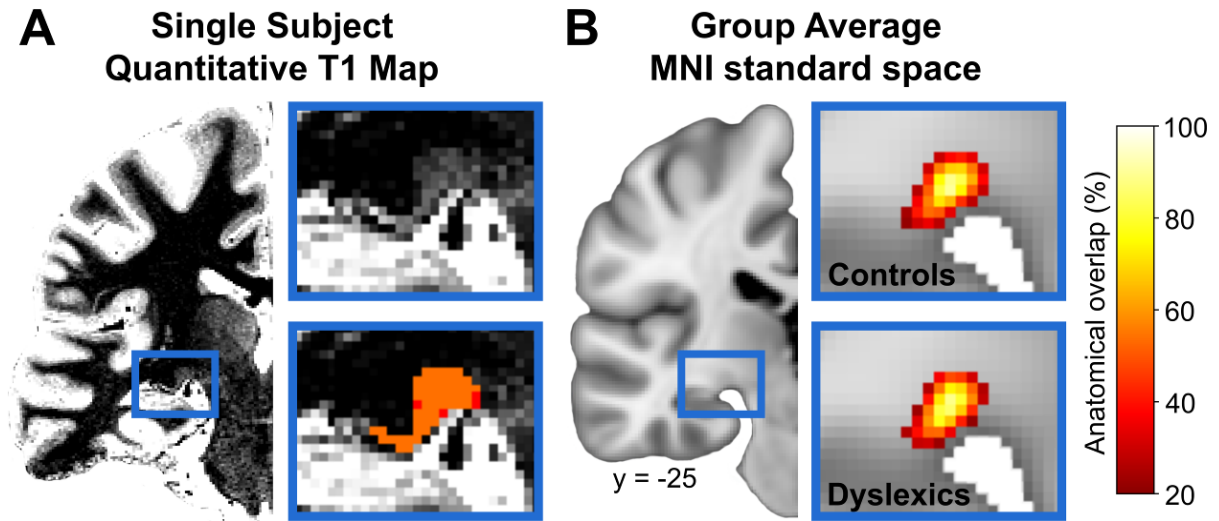


**Figure 1.** Manual segmentations of the left LGN. **A.** Left: Coronal view of the left hemisphere on the quantitative T<sub>1</sub> map of a representative single subject. The blue rectangle marks the region, which is shown at higher magnification in the two accompanying inserts. Top right insert: Enlarged view of the left LGN. Bottom right insert: Left LGN overlaid with a conjunction mask created from the manually segmented LGN masks by two independent raters. Orange color depicts voxels that were included by both raters. Red color depicts voxels that were only included by one of the two raters. Segmentations of both raters were merged for each participant, such that only those voxels that were segmented by both raters comprised the final LGN masks used for probabilistic tractography (orange color). The inter-rater reliability of these segmentations was high (mean dice coefficient: 0.86; see Supplemental Experimental Procedures). **B.** Left: Coronal view of the left hemisphere on the Montreal Neurological Institute (MNI) standard brain. The blue rectangle marks the region, which is shown at higher magnification in the two accompanying inserts. Top right insert: Group average map of the LGN masks in control participants (n=12) in MNI standard space. Bottom right insert: Group average map of the LGN masks in dyslexic participants (n=12) in MNI standard space. Group average maps were thresholded to show a minimum of 20% anatomical overlap across participants. Contrary to a previous report [62], there was no significance difference in LGN volume between the two groups [ $t(22) = .56$ ,  $P = .58$ ].

The direct V5/MT-LGN connection was clearly separate from the V1-LGN connection and was consistently located dorsal to the V1-LGN connection in both groups (Figure 3). On a first visual inspection the V5/MT-LGN pathway appeared weaker in dyslexic than in control participants (Figures 2B and 3).

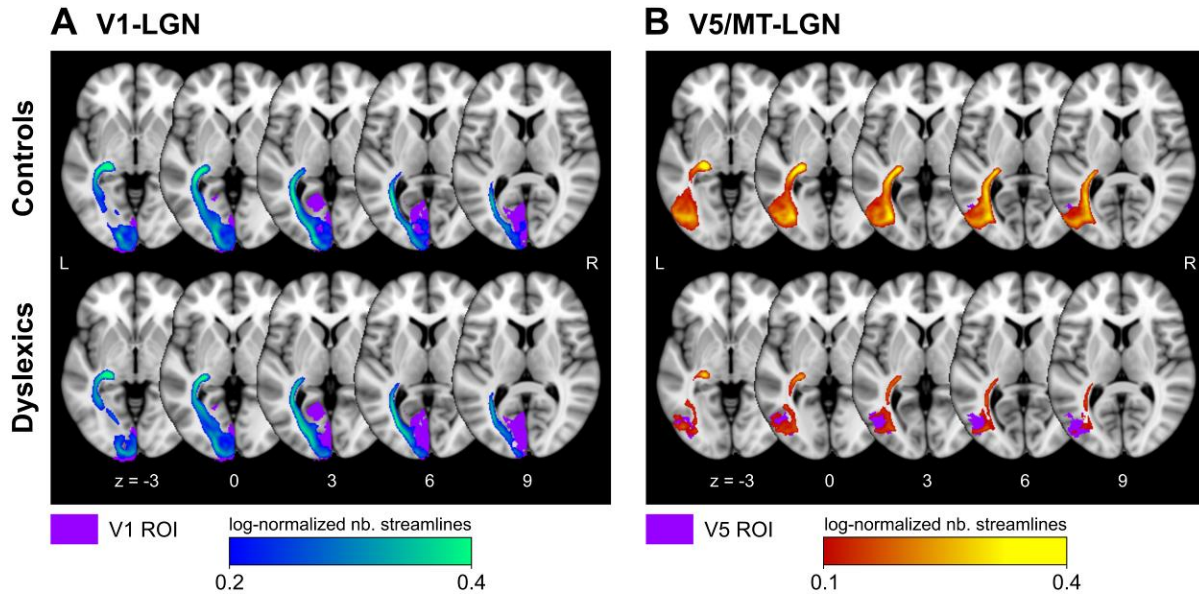


**Figure 2.** Two-dimensional representation of the left V1-LGN and V5/MT-LGN group averaged tracts in controls (n=12) and dyslexics (n=12) in MNI standard space. The group averaged tracts represent the mean probability and strength of a connection computed by the number of reconstructed streamlines per voxel (see Supplemental Experimental Procedures). **A.** Left V1-LGN connection in controls and dyslexics. Cortical seed area left V1 is indicated in purple. For visualization purposes, the group tracts were thresholded to show voxels with an average log-normalized number of streamlines per voxel of at least 0.2. **B.** Left V5/MT-LGN connection in controls and dyslexics. Cortical seed area left V5/MT is indicated in purple. Note that cortical seed area V5/MT is barely visible in control participants due to the large extent of resolved V5/MT-LGN streamlines in this group. For visualization purposes, the group tracts were thresholded to show voxels with an average log-normalized number of streamlines per voxel of at least 0.1. Numbers below images indicate z coordinates in MNI standard space.

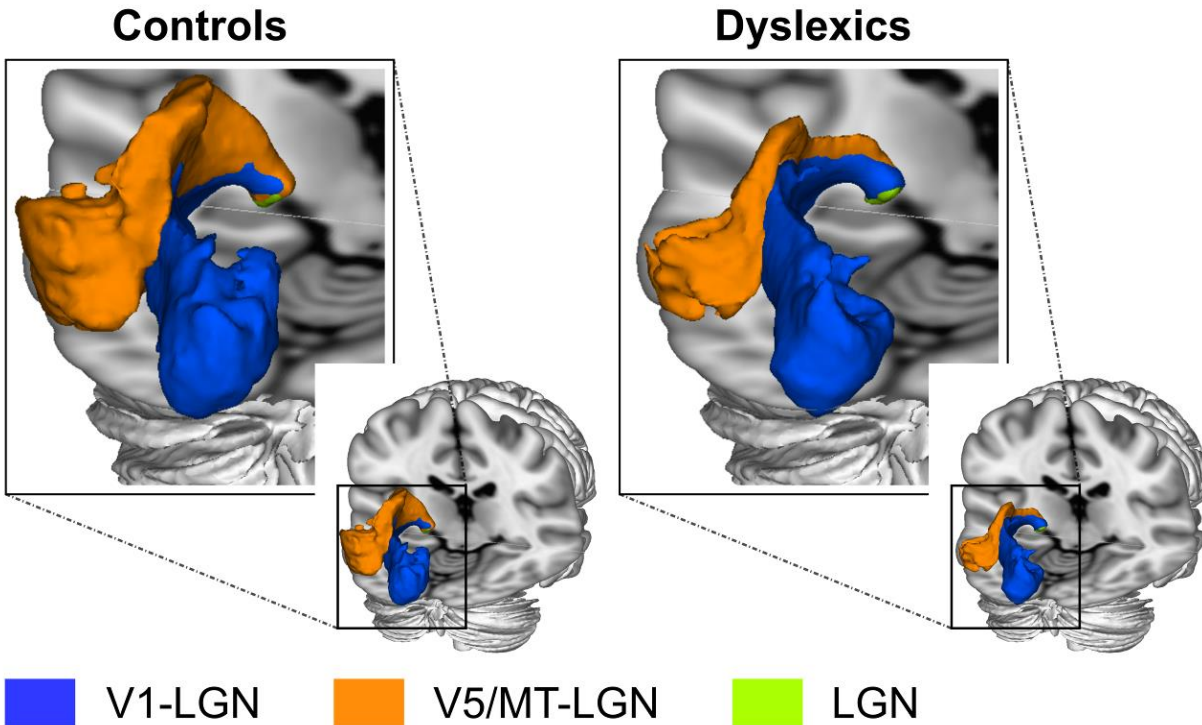


**Figure 3.** Three-dimensional representation of the left V1-LGN and V5/MT-LGN group averaged tracts in controls (n=12) and dyslexics (n=12) in MNI standard space. The group averaged tracts were thresholded to the same values as in Figure 2.

To formally test whether dyslexics have reduced left-hemispheric V1-LGN and V5/MT-LGN connections, we quantified the connection strength between the left LGN and visual cortical areas left V1 and V5/MT for each individual participant by means of a connectivity index. The connectivity index was defined as the log-normalized streamline count in the LGN target mask resulting from probabilistic tractography from cortical seed areas V1 and V5/MT.

A 2×2 mixed-model ANOVA on LGN connectivity indices with group (controls vs. dyslexics) as between-subjects factor and cortical seed area (V1 vs. V5/MT) as within-subjects factor (Figure 4A) showed a significant main effect of cortical seed area [ $F(1, 22) = 41.85, P < .001, \eta^2 = .61$ ], with higher connectivity indices for the connection left V1-LGN than the connection left V5/MT-LGN. This is in accordance with the fact that a vast majority of LGN neurons are connected with V1 [reviewed in refs. 18, 28]. In line with our hypothesis, we found a significant main effect of group, indicating a general reduction

in LGN connections in dyslexics as compared to controls [ $F(1, 22) = 4.28$ ,  $P = .05$ ,  $\eta^2 = .16$ ]. In addition, the analysis revealed a significant interaction between group and cortical seed area [ $F(1, 22) = 4.97$ ,  $P = .036$ ,  $\eta^2 = .07$ ]. Planned comparisons (one-tailed independent t-tests; Bonferroni corrected) showed that individuals with dyslexia had significantly lower connectivity indices for the connection left V5/MT-LGN as compared to controls [ $t(22) = 3.13$ ,  $P = .005$ ,  $d_s = 1.28$ ] (Figure 4A). Conversely, there was no difference in the connectivity indices for the left V1-LGN connection between controls and dyslexics [ $t(22) = .24$ ,  $P = .82$ ,  $d_s = .10$ ].

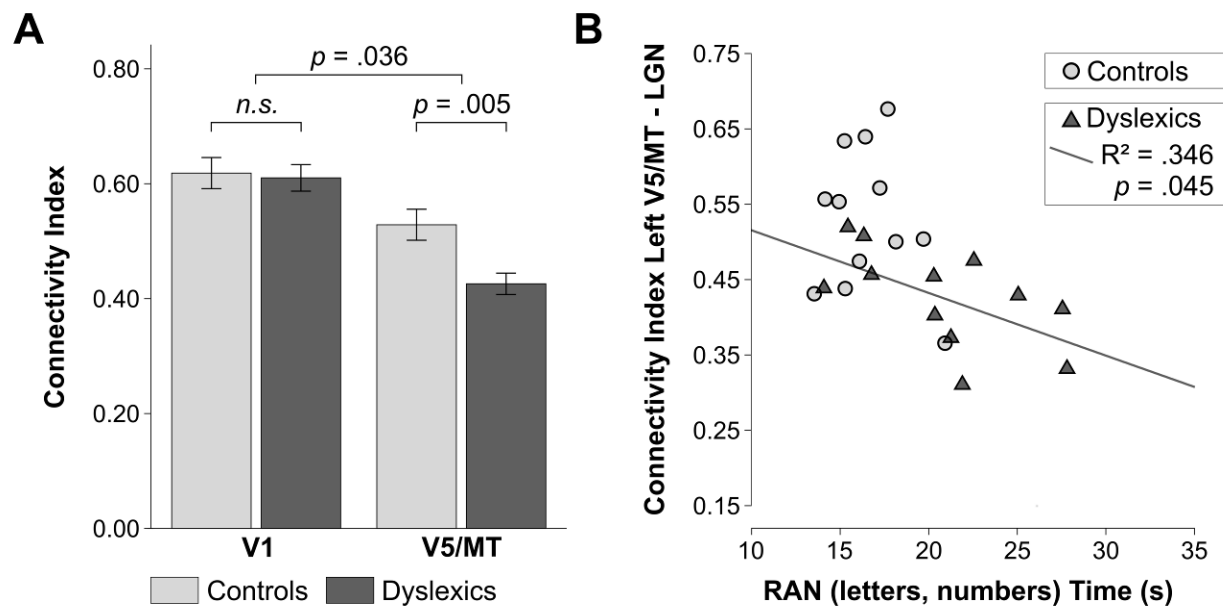


**Figure 4.** Structural connectivity of the LGN in the left hemisphere in controls ( $n=12$ ) and dyslexics ( $n=12$ ), and its behavioral relevance for a key dyslexia symptom. **A.** LGN connectivity indices in the left hemisphere in controls and dyslexics obtained from probabilistic tractography using a volume-based atlas for defining cortical seed areas V1 and V5/MT. Error bars represent  $\pm 1$  SEM. **B.** The strength of V5/MT-LGN connectivity correlated negatively with the time needed to rapidly name letters and numbers in dyslexic but not in control participants. Rapid naming abilities were measured with the standard diagnostic test for RAN [32].

The difference between dyslexic and control participants in the strength of left V5/MT-LGN connections cannot be explained by differences in the size of seed or target masks between groups. Firstly, we corrected the streamline count in the LGN target masks for the volume of the respective seed mask. Secondly, there was no significant difference in the mean volume of the LGN target masks [ $t(22) = .98$ ,  $P = .34$ ] nor the V5/MT seed masks [ $t(22) = -.11$ ,  $P = .92$ ] between groups (Table S2).

The finding of reduced structural connections in the direct left V5/MT-LGN pathway in dyslexics adds two fundamental novel contributions to the field. First, while Livingstone et al. [6] have shown histological alterations at the level of the LGN in several post-mortem cases with dyslexia, we here showed that the connections between the LGN and the cerebral cortex were reduced in dyslexics in-vivo. This finding is particularly interesting, because it parallels findings in animal models, where the induction of cortical microgyria, which are similar to those discovered in post-mortem brains of dyslexics, led to a severe reduction in thalamo-cortical and cortico-thalamic connections [11, reviewed in ref. 13]. Second, our study revealed a specific reduction in left-hemispheric cortico-subcortical connections between visual area V5/MT and the LGN in dyslexics, while the connections between V1 and the LGN were spared. Such a specific reduction is informative about the possible functional roles of structural alterations in the early visual pathway for dyslexia symptoms.

Most current theories on developmental dyslexia focus on the cerebral cortex to explain the etiology of this disorder [e.g., 13, 29-31]. These cortical models of dyslexia implicitly or explicitly assume that alterations of subcortical sensory structures are not causally related to key dyslexia symptoms. A prominent model of dyslexia proposes that subcortical sensory alterations as found in postmortem studies and animal models are not related to core traits of dyslexia, such as poor reading and slow naming of letters and numbers. Instead, subcortical sensory alterations are thought to solely explain sensory and motor symptoms that are only occasionally associated with developmental dyslexia [13]. Contrary to this assumption, it has recently been proposed that slow naming and poor reading comprehension in developmental dyslexia relates to sensory thalamus dysfunction [15]. To test these opposing hypotheses, we correlated participants' V5/MT-LGN connectivity indices with their reading comprehension scores as well as their composite scores on rapid automatized naming (RAN) [32] for letters and numbers. Our correlation analyses revealed, in dyslexic participants only, a significant negative correlation between the strength of left V5/MT-LGN connections



and the time needed to name letters and numbers aloud [ $R = -.588$ ,  $P = .045$ ; one-tailed Pearson's correlation, Bonferroni corrected for two tests] (Figure 4B). In control participants, there was no correlation with rapid naming abilities [ $R = -.202$ ,  $P = .530$ ] (Figure 4B). The significant correlation in dyslexics indicated that dyslexic participants with weaker V5/MT-LGN connections had more severe rapid naming deficits. There was no significant correlation between the strength of left V5/MT-LGN connections and participants' reading comprehension scores, neither in dyslexic [ $R = -.213$ ,  $P = .507$ ] nor in control participants [ $R = .076$ ,  $P = .814$ ]. The behavioral correlation between the strength of left-hemispheric V5/MT-LGN connections and a dyslexia diagnostic score (i.e. rapid naming ability) implies a behavioral relevance for V5/MT-LGN alterations for a core dyslexia symptom. Rapid naming performance is one of the strongest predictors of reading ability [33, 34, reviewed in ref. 14] and deficits in rapid naming ability present a core symptom of dyslexia in childhood throughout adolescence and in adulthood [33, 34, 35, reviewed in ref. 14].

One feature of studies with modest sample sizes is that the results are prone to variation based on minute analytical changes [36]. In a next step, we therefore aimed to reproduce the results of our tractography analysis using a surface-based approach [37] to define visual cortical areas V1 and V5/MT (see Supplemental Experimental Procedures). While volume-based atlases are widely used in diffusion MRI research [e.g., 38, 39, 40], surface-based atlases are thought to yield a higher anatomical mapping accuracy [37, 41, 42]. We found qualitatively the same results as with the volume-based atlases, i.e. a significant reduction of left-hemispheric V5/MT-LGN connections in dyslexics and a significant correlation of the connectivity strength of this pathway with rapid naming abilities in dyslexics only (see Figure S1, and Supplemental Experimental Procedures).

Area V5/MT is critical for the perception of visual motion [43, 44, reviewed in ref. 45]. Multiple studies have found aberrant motion perception in individuals with dyslexia and pre-readers at familial risk for the disorder [46-49]. In addition, targeted motion perception training improves reading ability in children and adults with dyslexia [47]. However, there are also indications that area V5/MT plays a role for rapid naming abilities: A recent transcranial direct current stimulation (tDCS) study in adult dyslexics showed that anodal stimulation of left area V5/MT (i.e., facilitating cortical V5/MT activity) resulted in a significant improvement in dyslexics' rapid naming abilities for numbers and a trend towards improvement for letters [50]. In addition, a structural MRI

study in a sample of pre-reading children with and without a family-history of dyslexia found that the grey matter volume of a left-hemispheric occipito-temporal region correlated with children's rapid naming abilities [51]. Crucially, the reported peak MNI coordinate of this left-hemispheric occipito-temporal region coincides with the anatomical location of area V5/MT. Our finding of a behavioral correlation between the strength of left-hemispheric V5/MT-LGN connections and rapid naming abilities in dyslexics suggests that dyslexia symptoms might not only be linked to area V5/MT or the visual dorsal stream but might be associated with alterations already present at the level of direct V5/MT-LGN connections.

An interesting question in light of the current findings regards the morphological origin of the reduced left-hemispheric V5/MT-LGN connections in dyslexics. Studies in non-human animals have shown that the direct (V1-bypassing) geniculate projections to area V5/MT originate predominantly in the koniocellular layers of the LGN [19, 21], with only occasional V5/MT relay cells also observed in parvocellular and magnocellular layers. In contrast, histological alterations in post-mortem brains of dyslexics have been observed specifically in the magnocellular layers of the LGN [6]. This apparent discrepancy might at least partly be explained by the fact that most of our current knowledge of the different geniculocortical pathways stems from studies in non-human mammals [reviewed in ref. 52]. As perfect homology between species cannot be assumed [53], it is theoretically possible that the direct LGN-V5/MT connection in humans also comprises strong magnocellular components. In addition, there is currently not much knowledge about the potential feedback connections from area V5/MT to the LGN in any species. There is evidence that thalamic response properties are heavily influenced by cortico-thalamic feedback [reviewed in ref. 54], and that such top-down modulation of early sensory structures is dysfunctional in individuals with dyslexia [15, 55]. In non-human primates, cortico-thalamic feedback from area V5/MT modulates early visual processing in magnocellular, parvocellular and koniocellular LGN cells [56, reviewed in ref. 57]. Thus, our findings could potentially reflect a reduction in feedback connections from left area V5/MT to the magnocellular layers of the LGN. However, at present this is speculative due to the rather low spatial resolution of diffusion-weighted MRI data and because probabilistic tractography does not give information about the direction of resolved connections.

The observed correlation between left V5/MT-LGN connectivity strength and rapid naming abilities in dyslexics was not predicted by purely cortical models of dyslexia [see

e.g. 13]. The result, however, converges well with recent findings in the auditory modality [15, 55, 58, 59]. Most important in the context of the present study, an fMRI study showed lower responses of the left auditory sensory thalamus (i.e., the medial geniculate body, MGB) in dyslexics as compared to controls for recognizing phonemes in contrast to other speech features [15]. Crucially, the amount of this task-dependent left MGB modulation predicted rapid naming abilities for letters and numbers in dyslexics. This previous fMRI and the present study together suggest that rapid naming difficulties in dyslexia are associated with aberrant function of the sensory thalamus and its connections. The findings imply that dyslexia might be best explained by a combination of cortical and subcortical sensory accounts of developmental dyslexia [e.g., 15, 55, 58-60] into a comprehensive cortico-subcortical framework.

## Conclusions

This study is the first to show structural alterations in visual subcortical sensory pathways in developmental dyslexia. Additionally, it gives important insight into the functional relevance of cortico-thalamic connections for developmental dyslexia, both because of the specificity of the reduction for the LGN-V5/MT connection as well as the behavioral correlation with a key symptom of dyslexia. Together with the few previous studies on subcortical sensory structures and function in dyslexia [6, 7, 15, 55, 58, 59], the results imply that the currently predominant approach to investigate dyslexia brain mechanisms solely at the cerebral cortex level might not be sufficient for a full understanding of key symptoms of the disorder [e.g., 30, 61, reviewed in refs. 4, 5]. Our study emphasizes the need and paves the way for unraveling the contributions of subcortical sensory pathways to dyslexia with sophisticated neuroimaging approaches with high spatial resolution. We expect that in the future such approaches will lead to a better understanding of dyslexia symptoms within a comprehensive cortico-subcortical framework.

**Authors Contributions.** C.M.A. and K.v.K. designed the experiment. C.M.A. and A.A. performed the experiment and analyzed the data. C.M.A. and K.v.K. wrote the manuscript.

**Acknowledgments.** We are grateful to our participants for their time and effort to participate in this study. We thank Morgan Blumberg for her contribution to the LGN segmentations. We thank Begoña Díaz, Domenica Wilfling, Elisabeth Wladimirow and Florian Hintz for providing the structural MRI data and the dyslexia diagnostic scores. We thank Stefan Kiebel for comments on an earlier version of the manuscript. The work was supported by a Max Planck Research Group grant and an ERC-Consolidator Grant (SENSOCOM, 647051) to K.v.K. The authors declare no competing financial interests.

## Methods

**Participants.** 24 adult German speakers were recruited for the current study. The sample included 12 participants with developmental dyslexia and 12 control participants (Table S1, and Supplemental Experimental Procedures). Both groups were matched in chronological age, sex, educational level, handedness and non-verbal IQ. Participants with dyslexia scored lower than controls on literacy tests involving spelling, reading speed, and comprehension as well as on rapid automatized naming (RAN) for letters and numbers (Table S1, and Supplemental Experimental Procedures).

**Data Acquisition of Ultra-High Resolution Anatomical Images.** Ultra-high resolution anatomical images were acquired on a 7 Tesla Magnetom MRI system (Siemens Healthineers, Erlangen, Germany) using a 24-channel head array coil (NOVA Medical Inc., Wilmington MA, USA). We employed a 3D MP2RAGE sequence [63] to acquire whole-brain images with an isotropic resolution of 700  $\mu\text{m}$ . The MP2RAGE sequence included two read-outs at different inversion times, from which a quantitative map of  $T_1$  relaxation times per voxel was calculated. These maps are well suited for brain segmentations as they provide excellent tissue contrast between white and gray matter [63]. For further details see Supplemental Experimental Procedures.

**Data Acquisition and Preprocessing of Diffusion-Weighted Images.** Diffusion-weighted images (dMRI) were acquired on a 3 Tesla Tim Trio MRI system with a 32-channel head coil (Siemens Healthineers, Erlangen, Germany) using a twice-refocused spin-echo echo-planar imaging (EPI) sequence (voxel size =  $1.72 \times 1.72 \times 1.7 \text{ mm}^3$ , 60 diffusion-encoding gradient directions,  $b = 1000 \text{ s/mm}^2$ ). Standard preprocessing of the dMRI data was done using the software packages LIPSIA (<http://www.cbs.mpg.de/>

institute/software/lipsia) and FSL (version 5.0, FMRIB Software Library, University of Oxford, <http://www.fmrib.ox.ac.uk/fsl>). For details see Supplemental Experimental Procedures.

### **Definition of Regions of Interest.**

*Left LGN.* The left lateral geniculate nucleus (LGN) was manually segmented on each participant's quantitative T<sub>1</sub> map by two independent raters (Figure 1A). Conjoined LGN masks (i.e., overlap between the segmentations of both raters) were then transformed to the diffusion images using a combination of linear and non-linear registrations computed with FSL (see Supplemental Experimental Procedures).

*Left V1 and V5/MT.* We first used a volume-based approach to define left primary visual cortex (V1) and left middle temporal area (V5/MT). In this approach, we used volume-based probabilistic atlases of left V1 and left V5/MT from the Juelich Histological Atlas [64], as implemented in FSL. Both atlases were thresholded such that the mean grey matter volume across all participants in dMRI data space matched previously reported volume estimates of V1 and V5/MT (Table S2, and Supplemental Experimental Procedures).

For the surface-based approach, we used surface-based maximum probability maps of left V1 and left V5/MT from a recently published and cross-validated atlas based on fMRI [37] (Table S2, and Supplemental Experimental Procedures).

**Probabilistic Tractography.** We computed voxel-wise estimates of the fiber orientation distribution [65] from the pre-processed dMRI data using FSL. We estimated the distribution of up to two fiber orientations for each voxel, given the b-value and resolution of the dMRI data [66]. Probabilistic tractography was performed in individual dMRI data space using FSL with default parameters. This produces an estimate of the probability and strength of the most likely location of a pathway [66]. We used modified Euler streamlining with the visual cortical areas (i.e., left V1 or V5/MT) as seeds and the participant-specific left LGN as both waypoint and termination mask to compute the connectivity between the LGN and the respective cortical area. All analyses were done separately for each pair of seed and target region. Tractography was only computed from the cortical region to the LGN to better detect possible non-dominant connections to the cortex, which might be missed by the algorithm when seeding in the LGN. In branching situations, probabilistic tractography has the tendency to miss the non-

dominant connection (false negative results), which can be reduced by seeding in cortical areas [67]. For details see Supplemental Experimental Procedures.

**Connectivity Index.** For each participant and pair of seed and target region, we computed a connectivity index,  $I$ , which was determined from the number of sample streamlines from each seed that reached the target [68]. As this number strongly depends on the number of voxels in the respective seed mask, we normalized the connectivity index,  $I$ , according to the following equation:

$$I = \frac{\log(\text{waytotal})}{\log(5000 \times V_{\text{seed}})} ,$$

wherein *waytotal* refers to the number of streamlines from a given seed that reached the target (i.e., numeric output of the tractography algorithm), *5000* refers to the number of generated sample streamlines in each seed voxel, and  $V_{\text{seed}}$  denotes the number of voxels in the respective seed mask. As the connectivity indices cannot be expected to be normally distributed across participants, we computed the logarithmic scaling (log) of each term of the equation to transform the connectivity index into a normally distributed variable (ranging between 0 and 1).

**Statistical Analyses.** For all statistical tests, the significance level  $\alpha$  was defined at 5% ( $p \leq .05$ ). All measures met the normality assumption as assessed with the Shapiro-Wilk test [69]. Effect sizes for ANOVAs were calculated using eta squared ( $\eta^2$ ) [70]. Effect sizes for independent t-tests were calculated using Cohen's  $d_s$  [71]. Analyses were carried out in Matlab (version 8.6, The MathWorks Inc., MA, USA) and IBM SPSS Statistics (version 22, IBM Corporation, NY, USA).

## References

1. Giraud, A.L., and Ramus, F. (2013). Neurogenetics and auditory processing in developmental dyslexia. *Curr Opin Neurobiol* 23, 37-42.
2. Peterson, R.L., and Pennington, B.F. (2012). Developmental dyslexia. *Lancet* 379, 1997-2007.
3. Norton, E.S., Beach, S.D., and Gabrieli, J.D. (2015). Neurobiology of dyslexia. *Curr Opin Neurobiol* 30, 73-78.
4. Vandermosten, M., Boets, B., Wouters, J., and Ghesquiere, P. (2012). A qualitative and quantitative review of diffusion tensor imaging studies in reading and dyslexia. *Neurosci Biobehav Rev* 36, 1532-1552.
5. Richlan, F. (2012). Developmental dyslexia: dysfunction of a left hemisphere reading network. *Front Hum Neurosci* 6, 120.
6. Livingstone, M.S., Rosen, G.D., Drislane, F.W., and Galaburda, A.M. (1991). Physiological and anatomical evidence for a magnocellular defect in developmental dyslexia. *Proc Natl Acad Sci U S A* 88, 7943-7947.
7. Galaburda, A.M., Menard, M.T., and Rosen, G.D. (1994). Evidence for aberrant auditory anatomy in developmental dyslexia. *Proc Natl Acad Sci U S A* 91, 8010-8013.
8. Herman, A.E., Galaburda, A.M., Fitch, R.H., Carter, A.R., and Rosen, G.D. (1997). Cerebral microgyria, thalamic cell size and auditory temporal processing in male and female rats. *Cereb Cortex* 7, 453-464.
9. Peiffer, A.M., McClure, M.M., Threlkeld, S.W., Rosen, G.D., and Fitch, R.H. (2004). Severity of focal microgyria and associated rapid auditory processing deficits. *Neuroreport* 15, 1923-1926.
10. Peiffer, A.M., Rosen, G.D., and Fitch, R.H. (2002). Rapid auditory processing and MGN morphology in microgyric rats reared in varied acoustic environments. *Dev Brain Res* 138, 187-193.
11. Rosen, G.D., Burstein, D., and Galaburda, A.M. (2000). Changes in efferent and afferent connectivity in rats with induced cerebrocortical microgyria. *J Comp Neurol* 418, 423-440.
12. Rosen, G.D., Mesples, B., Hendriks, M., and Galaburda, A.M. (2006). Histometric changes and cell death in the thalamus after neonatal neocortical injury in the rat. *Neuroscience* 141, 875-888.

13. Ramus, F. (2004). Neurobiology of dyslexia: a reinterpretation of the data. *Trends Neurosci* 27, 720-726.
14. Norton, E.S., and Wolf, M. (2012). Rapid Automatized Naming (RAN) and Reading Fluency: Implications for Understanding and Treatment of Reading Disabilities. *Annu Rev Psychol* 63, 427-452.
15. Diaz, B., Hintz, F., Kiebel, S.J., and von Kriegstein, K. (2012). Dysfunction of the auditory thalamus in developmental dyslexia. *Proc Natl Acad Sci U S A* 109, 13841-13846.
16. Jednorog, K., Marchewka, A., Altarelli, I., Monzalvo Lopez, A.K., van Ermingen-Marbach, M., Grande, M., Grabowska, A., Heim, S., and Ramus, F. (2015). How reliable are gray matter disruptions in specific reading disability across multiple countries and languages? Insights from a large-scale voxel-based morphometry study. *Hum Brain Mapp* 36, 1741-1754.
17. Andrews, T.J., Halpern, S.D., and Purves, D. (1997). Correlated size variations in human visual cortex, lateral geniculate nucleus, and optic tract. *J Neurosci* 17, 2859-2868.
18. Van Essen, D.C., Anderson, C.H., and Felleman, D.J. (1992). Information processing in the primate visual system: an integrated systems perspective. *Science* 255, 419-423.
19. Sincich, L.C., Park, K.F., Wohlgemuth, M.J., and Horton, J.C. (2004). Bypassing V1: a direct geniculate input to area MT. *Nat Neurosci* 7, 1123-1128.
20. Jayakumar, J., Roy, S., Dreher, B., Martin, P.R., and Vidyasagar, T.R. (2013). Multiple pathways carry signals from short-wavelength-sensitive ('blue') cones to the middle temporal area of the macaque. *J Physiol* 591, 339-352.
21. Warner, C.E., Goldshmit, Y., and Bourne, J.A. (2010). Retinal afferents synapse with relay cells targeting the middle temporal area in the pulvinar and lateral geniculate nuclei. *Front Neuroanat* 4, 8.
22. Bridge, H., Hicks, S.L., Xie, J.Y., Okell, T.W., Mannan, S., Alexander, I., Cowey, A., and Kennard, C. (2010). Visual activation of extra-striate cortex in the absence of V1 activation. *Neuropsychologia* 48, 4148-4154.
23. Bridge, H., Thomas, O., Jbabdi, S., and Cowey, A. (2008). Changes in connectivity after visual cortical brain damage underlie altered visual function. *Brain* 131, 1433-1444.
24. Lanyon, L.J., Giaschi, D., Young, S.A., Fitzpatrick, K., Diao, L., Bjornson, B.H., and Barton, J.J.S. (2009). Combined Functional MRI and Diffusion Tensor Imaging Analysis of Visual Motion Pathways. *J Neuro-Ophthalmol* 29, 96-103.



25. Gaglianese, A., Costagli, M., Bernardi, G., Ricciardi, E., and Pietrini, P. (2012). Evidence of a direct influence between the thalamus and hMT plus independent of V1 in the human brain as measured by fMRI. *Neuroimage* 60, 1440-1447.
26. Arrigo, A., Calamuneri, A., Mormina, E., Gaeta, M., Quartarone, A., Marino, S., Anastasi, G.P., and Aragona, P. (2016). New Insights in the Optic Radiations Connectivity in the Human Brain. *Invest Ophthalmol Vis Sci* 57, 1-5.
27. Skottun, B.C. (2015). The need to differentiate the magnocellular system from the dorsal stream in connection with dyslexia. *Brain Cogn* 95, 62-66.
28. Briggs, F., and Usrey, W.M. (2011). Corticogeniculate feedback and visual processing in the primate. *J Physiol* 589, 33-40.
29. Shaywitz, S.E., and Shaywitz, B.A. (2005). Dyslexia (specific reading disability). *Biol Psychiatry* 57, 1301-1309.
30. Boets, B., Op de Beeck, H.P., Vandermosten, M., Scott, S.K., Gillebert, C.R., Mantini, D., Bulthe, J., Sunaert, S., Wouters, J., and Ghesquiere, P. (2013). Intact but less accessible phonetic representations in adults with dyslexia. *Science* 342, 1251-1254.
31. Olulade, O.A., Napoliello, E.M., and Eden, G.F. (2013). Abnormal visual motion processing is not a cause of dyslexia. *Neuron* 79, 180-190.
32. Denckla, M.B., and Rudel, R.G. (1976). Rapid "automatized" naming (R.A.N): dyslexia differentiated from other learning disabilities. *Neuropsychologia* 14, 471-479.
33. Semrud-Clikeman, M., Guy, K., Griffin, J.D., and Hynd, G.W. (2000). Rapid naming deficits in children and adolescents with reading disabilities and attention deficit hyperactivity disorder. *Brain and Language* 74, 70-83.
34. Miller, C.J., Miller, S.R., Bloom, J.S., Jones, L., Lindstrom, W., Craggs, J., Garcia-Barrera, M., Semrud-Clikeman, M., Gilger, J.W., and Hynd, G.W. (2006). Testing the double-deficit hypothesis in an adult sample. *Ann Dyslexia* 56, 83-102.
35. Wolf, M., and Bowers, P.G. (1999). The double-deficit hypothesis for the developmental dyslexias. *J Educ Psychol* 91, 415-438.
36. Button, K.S., Ioannidis, J.P.A., Mokrysz, C., Nosek, B.A., Flint, J., Robinson, E.S.J., and Munafò, M.R. (2013). Power failure: why small sample size undermines the reliability of neuroscience. *Nat Rev Neurosci* 14, 365-376.
37. Wang, L., Mruczek, R.E., Arcaro, M.J., and Kastner, S. (2015). Probabilistic Maps of Visual Topography in Human Cortex. *Cereb Cortex* 25, 3911-3931.

38. Roberts, R.E., Bain, P.G., Day, B.L., and Husain, M. (2013). Individual differences in expert motor coordination associated with white matter microstructure in the cerebellum. *Cereb Cortex* 23, 2282-2292.
39. Floel, A., de Vries, M.H., Scholz, J., Breitenstein, C., and Johansen-Berg, H. (2009). White matter integrity in the vicinity of Broca's area predicts grammar learning success. *Neuroimage* 47, 1974-1981.
40. Caspers, S., Eickhoff, S.B., Rick, T., von Kapri, A., Kuhlen, T., Huang, R., Shah, N.J., and Zilles, K. (2011). Probabilistic fibre tract analysis of cytoarchitectonically defined human inferior parietal lobule areas reveals similarities to macaques. *Neuroimage* 58, 362-380.
41. Van Essen, D.C. (2005). A Population-Average, Landmark- and Surface-based (PALS) atlas of human cerebral cortex. *Neuroimage* 28, 635-662.
42. Hinds, O.P., Rajendran, N., Polimeni, J.R., Augustinack, J.C., Wiggins, G., Wald, L.L., Diana Rosas, H., Potthast, A., Schwartz, E.L., and Fischl, B. (2008). Accurate prediction of V1 location from cortical folds in a surface coordinate system. *Neuroimage* 39, 1585-1599.
43. Britten, K.H., Shadlen, M.N., Newsome, W.T., and Movshon, J.A. (1992). The analysis of visual motion: A comparison of neuronal and psychophysical performance. *J Neurosci* 12, 4745-4765.
44. Newsome, W.T., Britten, K.H., and Movshon, J.A. (1989). Neuronal Correlates of a Perceptual Decision. *Nature* 341, 52-54.
45. Zeki, S. (2015). Area V5-a microcosm of the visual brain. *Front Integr Neurosci* 9, 21.
46. Cornelissen, P., Richardson, A., Mason, A., Fowler, S., and Stein, J. (1995). Contrast Sensitivity and Coherent Motion Detection Measured at Photopic Luminance Levels in Dyslexics and Controls. *Vision Res* 35, 1483-1494.
47. Gori, S., Seitz, A.R., Ronconi, L., Franceschini, S., and Facoetti, A. (2016). Multiple Causal Links Between Magnocellular-Dorsal Pathway Deficit and Developmental Dyslexia. *Cereb Cortex* 26, 4356-4369.
48. Talcott, J.B., Hansen, P.C., Assoku, E.L., and Stein, J.F. (2000). Visual motion sensitivity in dyslexia: evidence for temporal and energy integration deficits. *Neuropsychologia* 38, 935-943.
49. Kevan, A., and Pammer, K. (2008). Visual deficits in pre-readers at familial risk for dyslexia. *Vision Res* 48, 2835-2839.

50. Heth, I., and Lavidor, M. (2015). Improved reading measures in adults with dyslexia following transcranial direct current stimulation treatment. *Neuropsychologia* 70, 107-113.
51. Raschle, N.M., Chang, M., and Gaab, N. (2011). Structural brain alterations associated with dyslexia predate reading onset. *Neuroimage* 57, 742-749.
52. Nassi, J.J., and Callaway, E.M. (2009). Parallel processing strategies of the primate visual system. *Nat Rev Neurosci* 10, 360-372.
53. Hickey, T.L., and Guillery, R.W. (1979). Variability of Laminar Patterns in Human Lateral Geniculate-Nucleus. *J Comp Neurol* 183, 221-246.
54. Saalmann, Y.B., and Kastner, S. (2011). Cognitive and Perceptual Functions of the Visual Thalamus. *Neuron* 71, 209-223.
55. Chandrasekaran, B., Hornickel, J., Skoe, E., Nicol, T., and Kraus, N. (2009). Context-Dependent Encoding in the Human Auditory Brainstem Relates to Hearing Speech in Noise: Implications for Developmental Dyslexia. *Neuron* 64, 311-319.
56. Jones, H.E., Andolina, I.M., Grieve, K.L., Wang, W., Salt, T.E., Cudeiro, J., and Sillito, A.M. (2013). Responses of primate LGN cells to moving stimuli involve a constant background modulation by feedback from area MT. *Neuroscience* 246, 254-264.
57. Sillito, A.M., Cudeiro, J., and Jones, H.E. (2006). Always returning: feedback and sensory processing in visual cortex and thalamus. *Trends in Neurosciences* 29, 307-316.
58. Hornickel, J., Skoe, E., Nicol, T., Zecker, S., and Kraus, N. (2009). Subcortical differentiation of stop consonants relates to reading and speech-in-noise perception. *Proc Natl Acad Sci U S A* 106, 13022-13027.
59. Banai, K., Hornickel, J., Skoe, E., Nicol, T., Zecker, S., and Kraus, N. (2009). Reading and subcortical auditory function. *Cereb Cortex* 19, 2699-2707.
60. Hari, R., and Renvall, H. (2001). Impaired processing of rapid stimulus sequences in dyslexia. *Trends Cogn Sci* 5, 525-532.
61. Perrachione, T.K., Del Tufo, S.N., Winter, R., Murtagh, J., Cyr, A., Chang, P., Halverson, K., Ghosh, S.S., Christodoulou, J.A., and Gabrieli, J.D. (2016). Dysfunction of Rapid Neural Adaptation in Dyslexia. *Neuron* 92, 1383-1397.
62. Giraldo-Chica, M., Hegarty, J.P., and Schneider, K.A. (2015). Morphological differences in the lateral geniculate nucleus associated with dyslexia. *Neuroimage Clin* 7, 830-836.

63. Marques, J.P., Kober, T., Krueger, G., van der Zwaag, W., Van de Moortele, P.F., and Gruetter, R. (2010). MP2RAGE, a self bias-field corrected sequence for improved segmentation and T1-mapping at high field. *Neuroimage* 49, 1271-1281.
64. Eickhoff, S.B., Stephan, K.E., Mohlberg, H., Grefkes, C., Fink, G.R., Amunts, K., and Zilles, K. (2005). A new SPM toolbox for combining probabilistic cytoarchitectonic maps and functional imaging data. *Neuroimage* 25, 1325-1335.
65. Behrens, T.E.J., Woolrich, M.W., Jenkinson, M., Johansen-Berg, H., Nunes, R.G., Clare, S., Matthews, P.M., Brady, J.M., and Smith, S.M. (2003). Characterization and propagation of uncertainty in diffusion-weighted MR imaging. *Magnet Reson Med* 50, 1077-1088.
66. Behrens, T.E.J., Berg, H.J., Jbabdi, S., Rushworth, M.F.S., and Woolrich, M.W. (2007). Probabilistic diffusion tractography with multiple fibre orientations: What can we gain? *Neuroimage* 34, 144-155.
67. Jones, D.K. (2010). Challenges and limitations of quantifying brain connectivity in vivo with diffusion MRI. *Imaging in Medicine* 2, 341-355.
68. Eickhoff, S.B., Jbabdi, S., Caspers, S., Laird, A.R., Fox, P.T., Zilles, K., and Behrens, T.E.J. (2010). Anatomical and Functional Connectivity of Cytoarchitectonic Areas within the Human Parietal Operculum. *J Neurosci* 30, 6409-6421.
69. Royston, P. (1992). Approximating the Shapiro-Wilk W-test for non-normality. *Statistics and Computing* 2, 117-119.
70. Cohen, J. (1973). Eta-Squared and Partial Eta-Squared in Fixed Factor Anova Designs. *Educ Psychol Meas* 33, 107-112.
71. Cohen, J. (1988). *Statistical Power Analysis for the Behavioral Sciences*, (New York, NY: Routledge Academic).

## Supplemental Data

**Table S1.** Demographic data and diagnostic tests for controls and dyslexics, related to Figure 1, and Figure 4B.

	Control group (n = 12)	Dyslexia group (n = 12)	Independent t- tests (df = 22)
Demographic data			
Mean age $\pm$ SD, years	23.7 $\pm$ 2.6	24.2 $\pm$ 2.4	NS
Male sex	12	12	—
No. right-handed	11	10	—
Education level	11 undergraduate students, 1 high school diploma	12 undergraduate students	—
Diagnostic tests, mean $\pm$ SD			
Nonverbal intelligence <sup>a</sup>	110.8 $\pm$ 12.8	101.0 $\pm$ 13.6	NS
Spelling <sup>b</sup>	102.8 $\pm$ 5.6	83.1 $\pm$ 7.6	$t = 7.2, P < .001$
Reading speed <sup>c</sup>	58.3 $\pm$ 9.1	42.6 $\pm$ 6.5	$t = 4.9, P < .001$
Reading comprehension <sup>c</sup>	62.9 $\pm$ 7.7	47.4 $\pm$ 4.2	$t = 6.1, P < .001$
RAN numbers			
Time (s)	16.8 $\pm$ 2.4	21.2 $\pm$ 6.1	$t = 2.3, P < .05$
Errors (%)	0.8 $\pm$ 1.3	0.2 $\pm$ 0.6	NS
RAN letters			
Time (s)	16.4 $\pm$ 2.6	20.3 $\pm$ 3.5	$t = 3.1, P < .01$
Errors (%)	0.3 $\pm$ 1.2	0.3 $\pm$ 0.8	NS

RAN = rapid automatized naming

<sup>a</sup>Raven matrices, scores based on standard scores (mean = 100, SD = 15).

<sup>b</sup>Spelling test, scores based on standard scores (mean = 100, SD = 10).

<sup>c</sup>Reading speed and comprehension tests, scores are based on t-standard scores (mean = 50, SD = 10).

**Table S2.** Left-hemispheric ROI volumes for controls and dyslexics in dMRI data space, related to Figure 1A, Figure 2, Figure 4, and Figure S1.

ROI volumes in mm <sup>3</sup> , mean $\pm$ SD	Control group (n = 12)	Dyslexia group (n = 12)	Independent t-tests (df = 22)
L LGN	132.4 $\pm$ 27.3	121.4 $\pm$ 27.5	$t = 0.98, P = .34$
Volume-based cortical ROIs			
L V1	6537.9 $\pm$ 915.7	6526.9 $\pm$ 686.7	$t = 0.03, P = .97$
L V5/MT	2753.6 $\pm$ 436.2	2775.6 $\pm$ 567.5	$t = 0.11, P = .92$
Surface-based cortical ROIs			
L V1	4407.6 $\pm$ 545.6	4361.5 $\pm$ 547.6	$t = 0.21, P = .84$
L V5/MT	911.0 $\pm$ 236.3	1004.5 $\pm$ 163.5	$t = 1.13, P = .27$

L = left

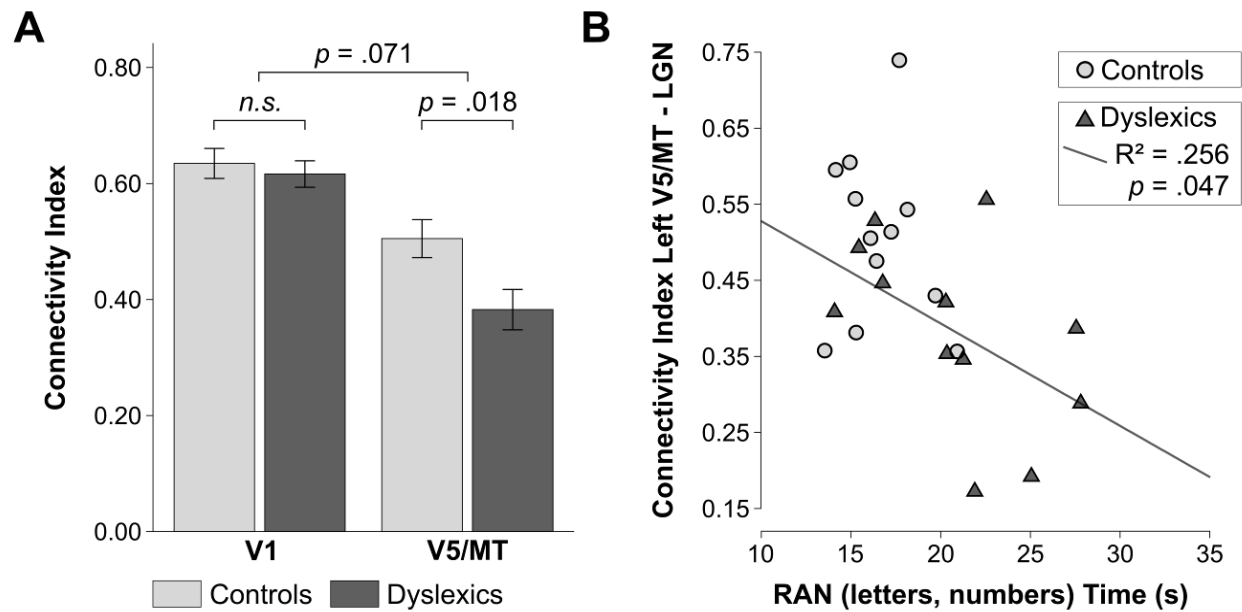


**Figure S1.** Results of the tractography analysis using a surface-based definition of cortical seed areas V1 and V5/MT (see Table S2), related to Figure 4.

Structural connectivity of the LGN in the left hemisphere in controls ( $n=12$ ) and dyslexics ( $n=12$ ), and its behavioral relevance for a key dyslexia symptom. **A.** LGN connectivity indices in the left hemisphere in controls and dyslexics obtained from running tractography using a surface-based atlas for defining cortical seed areas V1 and V5/MT. The LGN connectivity indices showed a high agreement with those obtained using the volume-based atlas for tractography: both for the connection left V1-LGN [ $R = .94$ ,  $P < .001$ ; one-tailed Pearson's correlation] and the connection left V5/MT-LGN [ $R = .83$ ,  $P < .001$ ; one-tailed Pearson's correlation]. A  $2 \times 2$  mixed-model ANOVA on the obtained LGN connectivity indices revealed a significant main effect of cortical seed area [ $F(1, 22) = 44.28$ ,  $P < .001$ ,  $\eta^2 = .63$ ], with higher connectivity indices for the connection left V1-LGN than the connection left V5/MT-LGN. The interaction between group and cortical seed area showed a trend towards significance [ $F(1, 22) = 3.6$ ,  $P = .071$ ,  $\eta^2 = .05$ ]. Planned comparisons (one-tailed independent t-tests; Bonferroni corrected) revealed the same pattern of simple effects as in the analysis with the volume-based atlases: dyslexic participants had significantly lower connectivity indices for the connection left V5/MT-LGN as compared to controls [ $t(22) = 2.55$ ,  $P = .018$ ,  $d_s = 1.04$ ], while there was no difference in the connectivity indices for the connection left V1-LGN [ $t(22) = .54$ ,  $P = .60$ ,  $d_s = .22$ ] between groups. Error bars represent  $\pm 1$  SEM. **B.** Consistent with the results of the volume-based analysis (Figure 4B), we found again that the strength of V5/MT-LGN connections correlated negatively with the time needed to rapidly name letters and numbers in dyslexic [ $R = -.506$ ,  $P = .047$ ] but not in control participants [ $R = -.141$ ,  $P = .331$ ].

## Supplemental Experimental Procedures

**Participants.** Written informed consent was obtained from all participants. The study was approved by the ethics committee of the Medical Faculty, University of Leipzig, Germany. All participants were native German speakers without a history of neurological and psychiatric disorders, and had been included in a previous fMRI study [S1]. Of the 14 participants in each group in the fMRI study, two dyslexics and one control subject were excluded from the present study because no diffusion MRI data could be obtained. An additional control subject was excluded because his non-verbal IQ, as assessed by

performance on the raven matrices [S2], was below the normal range (i.e., < 85). In the dyslexia group, 6 participants had a prior diagnosis of developmental dyslexia, while the other 6 participants reported having persistent reading and spelling problems since childhood. Group assignments were confirmed by tests on reading speed and comprehension [S3] and spelling [S4]. In addition, skills of rapid automatized naming (i.e., RAN for numbers and letters) [S5] were assessed. The scores on the diagnostic tests of dyslexia are summarized in Table S1.

**Data Acquisition of Ultra-High Resolution Anatomical Images.** Ultra-high resolution 7 Tesla MR images were acquired using a 3D MP2RAGE sequence with the following imaging parameters: 700  $\mu\text{m}$  isotropic resolution, TE = 3.04 ms, TR = 8250 ms,  $T_{11}$  = 1000 ms,  $T_{12}$  = 3300 ms, flip angle<sub>1</sub> = 7°, flip angle<sub>2</sub> = 5°, FOV = 224 × 224 × 168 mm<sup>3</sup>, GRAPPA acceleration factor = 2. The acquisition took approximately 13 minutes.

**Data Acquisition and Preprocessing of Diffusion-Weighted Images.** Diffusion-weighted MRI (dMRI) data were acquired using a twice-refocused spin echo-planar imaging (EPI) sequence [S6] with the following imaging parameters: voxel size = 1.72 × 1.72 × 1.7 mm<sup>3</sup>, TE = 100ms, TR = 12.9 s, FOV = 220 × 220 mm<sup>2</sup>, 88 axial slices covering the whole brain, no inter-slice gap. In addition, seven interspersed anatomical reference images without diffusion-weighting (b-value = 0 s/mm<sup>2</sup>) were obtained for off-line motion correction. The dMRI acquisition was accelerated using partial Fourier imaging (factor 6/8) and parallel imaging [GRAPPA; S7] with an acceleration factor of 2. Fat saturation was applied using a spectral saturation pulse. The dMRI sequence took approximately 16 min. In addition, a T<sub>1</sub>-weighted structural 3D image was acquired as anatomical reference on the same MRI system (MPRAGE, TE = 3.46 ms, TR = 1300 ms, TI = 650 ms, flip angle = 10°, 1 mm isotropic resolution, two averages). For preprocessing, the T<sub>1</sub>-weighted structural images were skull-stripped and rigidly aligned with the Talairach orientation [S8] using LIPSIA (<http://www.cbs.mpg.de/institute/software/lipsia>). To estimate motion correction parameters for the dMRI data, we used the seven reference images without diffusion-weighting and rigid-body registration [S9], implemented in FSL (FMRIB Software Library, University of Oxford <http://www.fmrib.ox.ac.uk/fsl>). Motion correction parameters were interpolated for all 67 volumes and combined with a global registration to the T<sub>1</sub> anatomy (in Talairach orientation) using rigid-body registration. The estimated motion correction parameters were then used to correct the gradient directions of each dMRI volume. The registered dMRI volumes were



sampled with an isotropic voxel resolution of 1.72 mm and the background was masked with the skull-stripped T<sub>1</sub>-image. Finally, a diffusion tensor was fit to each voxel and fractional anisotropy (FA) maps were computed.

**Manual Segmentations of the left Lateral Geniculate Nucleus.** Individual ultra-high resolution 7 Tesla MRI quantitative T<sub>1</sub> maps were used to manually segment the left LGN in each participant (Figure 1A). In coronal view, the LGN is ventrally adjoined by the hippocampal sulcus (cerebral spinal fluid, CSF). Dorsolaterally, the LGN is surrounded by the white matter fibers that form the triangular area (zone of Wernicke) [S10]. Given the lower T<sub>1</sub> relaxation times of the surrounding white matter and the high T<sub>1</sub> relaxation times of CSF [S11], the LGN can be clearly distinguished on quantitative T<sub>1</sub> maps. Manual segmentations were performed in FSLView (<http://fsl.fmrib.ox.ac.uk/fsl/fslview>) by two independent raters who were both blind to participants' group assignment.

*Standardized segmentation procedure.* In order to standardize the segmentation procedure between raters and across participants, we first computed the histogram of T<sub>1</sub> relaxation times for each participant (number of bins = 1000, bin size = 4). This yielded clear peaks of T<sub>1</sub> relaxation times in grey and white matter for each participant. We then loaded the MRI volume of each participant in the viewer and set the minimum intensity to half a standard deviation below the individual white matter relaxation time peak, while the maximum intensity was set to half a standard deviation above the individual grey matter T<sub>1</sub> relaxation time peak (corresponding to 88% of the peak T<sub>1</sub> relaxation time intensities assuming a Gaussian normal distribution). This was done to optimize the visibility of the LGN. Segmentations were then performed in coronal view aided by the sagittal and transverse views. All segmentations were performed in randomized order across participants. Finally, the LGN masks of both raters were conjoined, such that the final LGN masks only comprised those voxels that were segmented by both raters (Figure 1A).

*Inter-rater reliability.* Inter-rater reliability for the manual LGN segmentations was assessed by computing the dice coefficient as twice the amount of shared voxels between both raters' LGN masks divided by the total number of voxels in both masks:  $(2 \times \text{mask}_1 \cap \text{mask}_2) / (\text{mask}_1 + \text{mask}_2)$ , wherein mask<sub>1</sub> and mask<sub>2</sub> refer to the LGN masks of rater 1 and rater 2, respectively [S12]. The obtained coefficient yields a measure of the amount of agreement between the two raters and ranges from 0 (no agreement) to 1 (perfect agreement). The agreement between raters was high – both for

the LGN segmentations in control participants ( $0.86 \pm 0.04$ , mean  $\pm$  SD) as well as in dyslexic participants ( $0.85 \pm 0.04$ ).

*Registrations to individual dMRI data.* Conjoined LGN masks were registered to the individual dMRI data using a combination of linear and non-linear registrations computed with FSL. To facilitate registration accuracy, we used the individual co-registered skull-stripped uniform images of the MP2RAGE sequence rather than the quantitative  $T_1$  maps as input for these registrations. The  $T_1$ -weighted structural images (aligned with the dMRI data) served as registration target. The LGN masks were then warped into the individual space of the dMRI data by applying the obtained linear and non-linear registration parameters. All registrations were visually inspected for misalignments. Finally, the registered individual LGN masks were thresholded at an intensity of 0.4 (after linear interpolation to the target image) to preserve the volumes of the conjoined LGN masks. The group-specific LGN mask volumes after registration and thresholding are summarized in Table S2.

*Registrations to MNI standard space.* For visualization purposes, we normalized the unthresholded conjoined LGN masks in dMRI data space to MNI standard space (using the MNI 1 mm brain template as reference) and averaged the LGN masks within each group to derive a voxel-wise probability map of anatomical overlap across participants (Figure 1B).

### **Definition of Cortical Regions of Interest (ROI).**

*Volume-based definition of left V1 and V5/MT.* We derived probabilistic atlases of left primary visual cortex (V1) and left extrastriate visual area V5/MT from the Juelich Histological Atlas [S13], as implemented in FSL. Both probabilistic atlases were in MNI standard space with a voxel size of  $1 \text{ mm}^3$ .

The unthresholded probabilistic atlases of area V1 [S14] and V5/MT [S15, S16] cover large spatial extents due to the inter-individual anatomical variability of these areas. We therefore used the following procedure to find appropriate thresholds for the probabilistic atlases to confine the final left V1 and left V5/MT ROIs to anatomically plausible volumes: we first thresholded the probabilistic atlases at different percentages of overlap in steps of 5% from 5% to 95%. We then transformed all of these differently thresholded V1 and V5/MT atlases to each participant's dMRI data. We therefore registered the MNI 1 mm brain template to the individual  $T_1$ -weighted structural

images, which were aligned with the diffusion weighted images. Linear and non-linear registration was performed with FSL using default parameters. The probabilistic atlases were then warped to the individual dMRI data by applying the obtained linear and non-linear registration parameters. Next, the gray-matter areas of the registered V1 and V5/MT maps were computed using voxels inside the brain with FA < 0.2 defined from the diffusion image to guarantee a good quality mask for tractography. Finally, the remaining mean gray matter volumes of the atlases across all participants for each initial threshold were compared to anatomical volume estimates of left V1 and left V5/MT that have been reported in the literature, and the threshold that most closely corresponded to the reported volume estimate of the respective brain area was selected.

Based on post-mortem measurements, Andrews et al. [S17] reported volumes of left V1 = 3185 - 7568 mm<sup>3</sup>. We focused on the high end of the reported V1 volume range to assure that all voxels that are part of area V1 were included in the individual V1 ROIs and to partially account for volumetric tissue shrinkage in post-mortem preparations [S18]. We therefore chose a threshold of 60 % for the probabilistic atlas of left V1, which resulted in a mean volume of left V1 = 6532 ± 792 mm<sup>3</sup> across participants in dMRI data space. The group-specific left V1 ROI volumes are summarized in Table S2 (volume-based cortical ROIs).

Using a functional localizer, Bridge et al. [S19] reported a volume of 2500 mm<sup>3</sup> for area V5/MT. We therefore chose a threshold of 10 % for the probabilistic atlas of left V5/MT, which resulted in a mean volume of left V5/MT = 2765 ± 495 mm<sup>3</sup> across participants in dMRI data space. The group-specific volume-based left V5/MT ROI volumes are summarized in Table S2 (volume-based cortical ROIs).

The comparably great difference in chosen threshold for left V5/MT (10%) and left V1 (60%) atlases can be explained by a greater inter-individual structural variability in V5/MT location compared to V1 location. The maximum anatomical overlap in the probabilistic atlas of left V5/MT is 54% as compared to 100% for left V1.

*Surface-based definition of left V1 and V5/MT.* Surface-based atlases of left V1 and left V5/MT were derived from a recently published and cross-validated atlas based on fMRI [S20]. We used the provided maximum probability maps (i.e., indicating the most probable region for any given point) instead of the full probability maps (i.e., indicating the likelihood that a given point is part of any region) in order to avoid probability and thus volume thresholding. As the surface-based atlas features separate maximum

probability maps of both ventral and dorsal left V1, these two maps were conjoined to obtain a surface-based map covering entire left V1.

In order to map the surface-based atlases of V1 and V5/MT on each individual subject, we first reconstructed each participant's cortical surface using the software freesurfer (<https://surfer.nmr.mgh.harvard.edu/>). Each participant's skull-stripped T<sub>1</sub> image (aligned with the diffusion data) served as input for the reconstruction process. Subsequently, cortical surfaces were imported into the software AFNI (<https://afni.nimh.nih.gov/>) and resampled to match the template brain surface of the atlas using @SUMA\_Make\_Spec\_FS. Left V1 and V5/MT maximum probability labels were then mapped onto the individual surfaces and vertex coordinates of the labeled surface points were converted into voxel coordinates and marked in the individual brain volume. The surface-based masks were then dilated by one voxel (1 mm) in each dimension. This was done to facilitate tractography by ensuring closer proximity of the surface-based V1 and V5/MT ROIs to the surrounding white matter. Finally, the surface-based V1 and V5/MT ROIs were resampled to match the resolution of the diffusion data. This procedure resulted in a mean volume of left V1 =  $4385 \pm 535 \text{ mm}^3$  and left V5/MT =  $958 \pm 204 \text{ mm}^3$  across participants in dMRI data space. The group-specific surface-based left V1 and left V5/MT ROI volumes are summarized in Table S2 (surface-based cortical ROIs).

### **Probabilistic Tractography.**

*Tracking consistency.* To evaluate whether connections were consistently resolved in each participant, they had to meet three criteria: first, we evaluated the spatial consistency of the resolved connections across participants by visual inspection. This was done to assure that the reconstructed pathways followed the known anatomical literature priors [see e.g. S21]. Second, for the binary decision whether a specific connection was strong enough to be reliably detected by tractography, we regarded a connection between two brain areas as detected if at least 10 of the generated sample streamlines in a given seed region reached the target [S22]. Finally, we computed the mean and standard deviation (SD) of the connectivity indices (i.e., log-normalized streamline counts) for both the left-hemispheric V1-LGN and V5/MT-LGN connection separately for each group. A connection of a participant was considered inconsistent if his or her connectivity index was  $> 2.5$  SDs away from the group mean connectivity

index for the respective connection. All three criteria were fulfilled for each participant and each connection considered in this study.

*Group averaged tracts.* The output images of the probabilistic tractography for each connection (visitation maps) were normalized by logarithmic transformation (of all values  $> 0$ ) and division by the logarithm (log) of the total number of generated streamlines in each seed mask. This was the same normalization procedure as described in detail in the Methods for the connectivity indices. The resulting images contained the log-normalized number of streamlines per voxel, scaled between 0 and 1. The log transformation helped to approach a Gaussian normal distribution of the initially not normally distributed visitation values and is mandatory for the normalization to the MNI 1 mm brain template, which includes linear interpolation. In MNI space, each connection was averaged within controls and dyslexics to derive group averaged tracts for left-hemispheric V1-LGN and V5/MT-LGN connections (Figure 2 and Figure 3).

## Supplemental References

- S1. Diaz, B., Hintz, F., Kiebel, S.J., and von Kriegstein, K. (2012). Dysfunction of the auditory thalamus in developmental dyslexia. *Proc Natl Acad Sci U S A* 109, 13841-13846.
- S2. Raven, J.C. (1998). *Advanced progressive matrices*, (Oxford, UK: Oxford Psychologists Press).
- S3. Schneider, W., Schlagmüller, M., and Ennemoser, M. (2007). *Lesegeschwindigkeits- und verständnistest für die Klassen 6-12*, (Göttingen, Germany: Hogrefe).
- S4. Kersting, M., and Althoff, K. (2004). *Rechtschreibungstest*, (Göttingen, Germany: Hogrefe).
- S5. Denckla, M.B., and Rudel, R.G. (1976). Rapid "automatized" naming (R.A.N): dyslexia differentiated from other learning disabilities. *Neuropsychologia* 14, 471-479.
- S6. Reese, T.G., Heid, O., Weisskoff, R.M., and Wedeen, V.J. (2003). Reduction of eddy-current-induced distortion in diffusion MRI using a twice-refocused spin echo. *Magn Reson Med* 49, 177-182.
- S7. Griswold, M.A., Jakob, P.M., Heidemann, R.M., Nittka, M., Jellus, V., Wang, J., Kiefer, B., and Haase, A. (2002). Generalized autocalibrating partially parallel acquisitions (GRAPPA). *Magn Reson Med* 47, 1202-1210.

- S8. Talairach, J., and Tournoux, P. (1988). Co-planar stereotaxic atlas of the human brain. 3-Dimensional proportional system: an approach to cerebral imaging., (Stuttgart: Thieme Medical Publishers).
- S9. Jenkinson, M., Bannister, P., Brady, M., and Smith, S. (2002). Improved optimization for the robust and accurate linear registration and motion correction of brain images. *Neuroimage* 17, 825-841.
- S10. Mai, J.K., and Paxinos, G. (2008). *Atlas of the Human Brain*, (Academic Press).
- S11. Wright, P.J., Mougin, O.E., Totman, J.J., Peters, A.M., Brookes, M.J., Coxon, R., Morris, P.E., Clemence, M., Francis, S.T., Bowtell, R.W., et al. (2008). Water proton T1 measurements in brain tissue at 7, 3, and 1.5 T using IR-EPI, IR-TSE, and MPRAGE: results and optimization. *MAGMA* 21, 121-130.
- S12. Dice, L.R. (1945). Measures of the Amount of Ecologic Association between Species. *Ecology* 26, 297-302.
- S13. Eickhoff, S.B., Stephan, K.E., Mohlberg, H., Grefkes, C., Fink, G.R., Amunts, K., and Zilles, K. (2005). A new SPM toolbox for combining probabilistic cytoarchitectonic maps and functional imaging data. *Neuroimage* 25, 1325-1335.
- S14. Amunts, K., Malikovic, A., Mohlberg, H., Schormann, T., and Zilles, K. (2000). Brodmann's areas 17 and 18 brought into stereotaxic space - Where and how variable? *Neuroimage* 11, 66-84.
- S15. Malikovic, A., Amunts, K., Schleicher, A., Mohlberg, H., Eickhoff, S.B., Wilms, M., Palomero-Gallagher, N., Armstrong, E., and Zilles, K. (2007). Cytoarchitectonic analysis of the human extrastriate cortex in the region of V5/MT+: A probabilistic, stereotaxic map of area h0c5. *Cereb Cortex* 17, 562-574.
- S16. Wilms, M., Eickhoff, S.B., Specht, K., Amunts, K., Shah, N.J., Malikovic, A., and Fink, G.R. (2005). Human V5/MT+: comparison of functional and cytoarchitectonic data. *Anat Embryol* 210, 485-495.
- S17. Andrews, T.J., Halpern, S.D., and Purves, D. (1997). Correlated size variations in human visual cortex, lateral geniculate nucleus, and optic tract. *J Neurosci* 17, 2859-2868.
- S18. Schulz, G., Crooijmans, H.J.A., Germann, M., Scheffler, K., Muller-Gerbl, M., and Muller, B. (2011). Three-dimensional strain fields in human brain resulting from formalin fixation. *J Neurosci Meth* 202, 17-27.
- S19. Bridge, H., Thomas, O., Jbabdi, S., and Cowey, A. (2008). Changes in connectivity after visual cortical brain damage underlie altered visual function. *Brain* 131, 1433-1444.

- S20. Wang, L., Mruczek, R.E., Arcaro, M.J., and Kastner, S. (2015). Probabilistic Maps of Visual Topography in Human Cortex. *Cereb Cortex* 25, 3911-3931.
- S21. Arrigo, A., Calamuneri, A., Mormina, E., Gaeta, M., Quartarone, A., Marino, S., Anastasi, G.P., and Aragona, P. (2016). New Insights in the Optic Radiations Connectivity in the Human Brain. *Invest Ophthalmol Vis Sci* 57, 1-5.
- S22. Blank, H., Anwender, A., and von Kriegstein, K. (2011). Direct Structural Connections between Voice- and Face-Recognition Areas. *J Neurosci* 31, 12906-12915.